DESIGN OF A SIX-AXIS PARALLEL NANOPOSITIONER USING DECOUPLED FLEXURAL LEGS

Chenglin Li, Xiangbo Liu and Shih-Chi Chen*
Department of Mechanical and Automation Engineering
The Chinese University of Hong Kong
Shatin, N.T., Hong Kong SAR, China
*Email: scchen@mae.cuhk.edu.hk

In this paper, we present the design of a compliant six-axis parallel nanopositioner. The mechanism is designed based on a new method of decoupled flexural legs. The nanopositioner is actuated by six linear actuators, located below flexure mechanism on the same plane, achieving a compact device envelope. Static and dynamic positioning experiments have been devised and performed to characterize the range, resolution, and speed characteristics of the nanopositioner.

PARALLEL FLEXURE STAGES

Nanopositioners can move objects of different sizes and scales with nanometer level precision. Nanopositioners are important as they set limits on our ability to measure, manipulate, and manufacture physical systems. To realize nanometer level repeatability and precision, flexure bearings or compliant mechanisms are often used for their advantages (e.g., no wear between joint members and free of backlash etc.) over traditional mechanical linkages [1].

Nanopositioners often operate in multiple axes, thereby controlling the position and/or orientation of an object in one to six degrees of freedom (DOF). Many commercial multi-DOF nanopositioners achieve the required DOFs by serially stacking up single-axis stages. Although this design approach is straightforward and typically has a larger work space, the positioner becomes tall and bulky with compromised resolution due to high temperature sensitivity. On the other hand, multi-DOF nanopositioners can be designed in a parallel fashion, making the positioner compact, light-weight with improved dynamic performance. The parallel nanopositioners are usually custom-designed owing to their limited range, load capacity, and complex control solution.

In recent years, many multi-DOF parallel positioners have been developed for various applications. Two design methods are frequently used to develop such systems: (1) constraint-based design (CBD) [2], and (2) pseudo-rigid-body model (PRBM) [1]. For example, based on CBD, the HexFlex mechanism is developed, i.e., a monolithic six-axis compliant stage that can be easily fabricated via waterjet or wire electrical discharge machining (EDM). However, three custom-designed two-axis voice coil actuators are required to drive the HexFlex mechanism [3,4]. Using PRBM, a Stewart platform [5] can be transformed into a six-axis compliant stage driven by six linear actuators. Nevertheless, its 3-D flexural joints are difficult and expensive to fabricate [6]. In this paper, we present a new compliant mechanism design method based on decoupled flexural legs, demonstrated with a six-axis nanopositioner with improved performance.

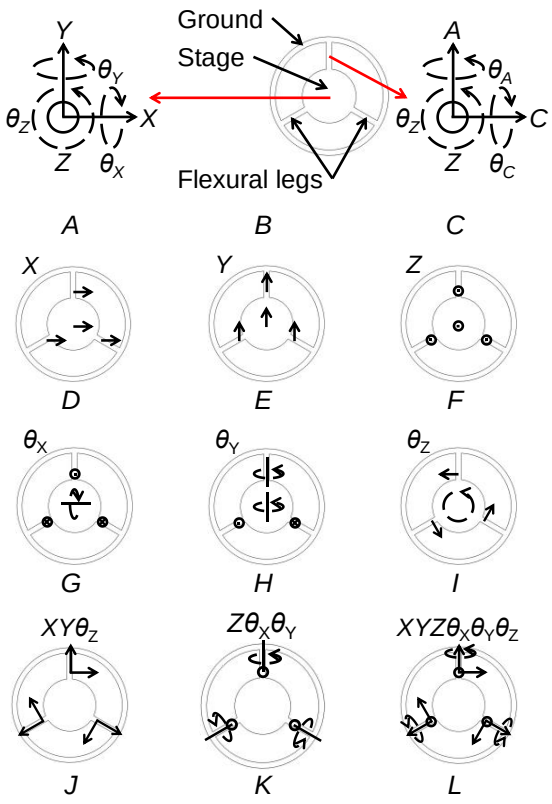

FIGURE 1. Schematic of a parallel flexure stage (B), consisting of a central stage and three flexural legs; global (A) and local (C) coordinates

set at the central stage and each leg respectively. Illustration of the motion decomposition (D~I) and composition (J~L)

Fig. 1B shows the schematic diagram of a parallel flexure stage, which consists a central stage, three equally-spaced flexural legs, and ground. The number of flexural legs (n) can be two or more depending on the design requirements. The global coordinate (Fig. 1A) is set at the central stage, and each flexural leg has a local coordinate (Fig. 1C), where A and C indicate the axial and circumferential directions, respectively. Fig. 1D - 1I illustrate the decomposition of the stage motions in all six axes, and notably only motions in the C, A, Z, and θ_A axes (in the local coordinates) are required for the flexural legs. Fig. 1J - 1L show examples of the multi-axis motion composition. For a six-DOF flexural stage (Fig. 1L), the flexural legs should have motions in the C, A, Z, and θ_A axes, while the θ_A DOF can be neglected as n (n ≥ 3) equally-spaced flexural legs with the Z DOF can achieve three out-of-plane rotations, e.g., rotations about different in-plane axes. Thus, flexural legs with three translational DOFs (TDOFs) are required to design six-axis parallel flexural stages.

DECOUPLED FLEXURAL LEGS

Generally, the design of appropriate flexural legs is the key step in designing a parallel mechanism. Here, we introduce a systematic approach to design multi-TDOF flexural legs by serially combining single-TDOF flexures. First, for one-TDOF flexural legs, we have the cantilever beam (CB), Fig. 2A, parallelogram (PA), Fig. 2B, and double parallelogram (DP), Fig. 2C, which are frequently used in CBD [7]. Besides, two additional one-TDOF flexures are considered, i.e., two cantilever beams joined collinearly at two fixed ends (CF), Fig. 2D, or two free ends (CC), Fig. 2E. As such, by serially combining the five different one-TDOF flexures, several different two-TDOF flexural legs and numerous three-TDOF flexural legs can be obtained. It is worthwhile to note that not all the generated flexural legs are suitable for fabrication and motion transfer. By using finite element analysis (FEA), we can determine best the flexural legs for different design requirements.

Figure 2 presents examples of two-TDOF or three-TDOF flexural legs: CC-CB (Fig. 2F~G), CB-CC (Fig. 2H~I), CB-CC-CB (Fig. 2J - 2L), and CB-CC-CF (Fig. 2M - 2O). To some extent, these flexural legs are “decoupled” due to the serial nature of the combination.

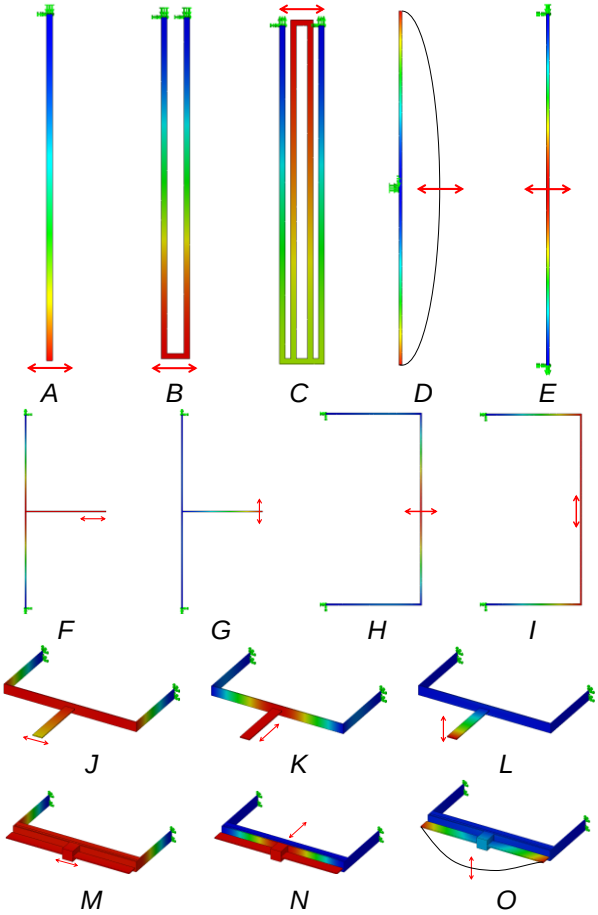

FIGURE 2. Examples of one-TDOF (A - E), two-TDOF (F - I), and three-TDOF (J - O) flexural legs

We can also analyze some of the existing parallel flexural stages using “flexural legs” concept. For example, the XY stage developed by Awtar [8] uses four DP-DP flexural legs, the HexFlex mechanism [3] uses three CC-CB flexural legs, and the μHexFlex mechanism [4] uses three CB-CC flexural legs. The reason that the HexFlex and μHexFlex can utilize three two-TDOF flexural legs to generate six-axis motions is that the width and thickness of the flexural beams have close values; as such the flexural legs are able to provide three TDOFs.

SIX-AXIS PARALLEL NANOPOSITIONER

To design a compact six-axis parallel nanopositioner, we first consider the best structure for actuation, and the CB-CC-CF flexural legs configuration (Fig. 2M - 2O) is selected. Fig. 3A presents the top view, global coordinate, and actuator layout of the six-axis parallel flexural stage, where actuators V_{C1}, V_{C2}, and V_{C3} are for in-plane motions ($X/Y/\theta_Z$), and actuators V_{Z1}, V_{Z2}, and V_{Z3} are for out-of-plane motions ($Z/\theta_X/\theta_Y$). Fig. 3B - 3G present the FEA

simulated results, which yields decoupled motions in all six axes, i.e., X, Y, Z, θ_X, θ_Y, and θ_Z. From the simulation, we can see that the in-plane and out-of-plane motions of the central stage are entirely decoupled.

Fig. 4C presents the CAD model of the six-axis parallel positioner, where the flexural stage is driven by six voice coil actuators (VCA) (NCC15-24-090-1X, H2W). The VCAs are used due to their high bandwidth (284 Hz) and high force output (18.1 N/amp). A decoupler mechanism (Fig. 4A) is affixed to the VCA, in order to ensure a pure Z motion input can be generated. A steering mechanism (Fig. 4B) is designed to transform the vertical motion into in-plane motion, allowing all VCAs to be positioned below the flexure stage. As shown in Fig. 4D, six capacitance probes are used to monitor the displacement of the central stage in all six axes in real time.

Figure 4D presents the prototype of six-axis nanopositioner with integrated actuators and sensors. The flexural stage is fabricated by wire-EDM and milling and made of 7075 aluminum alloy.

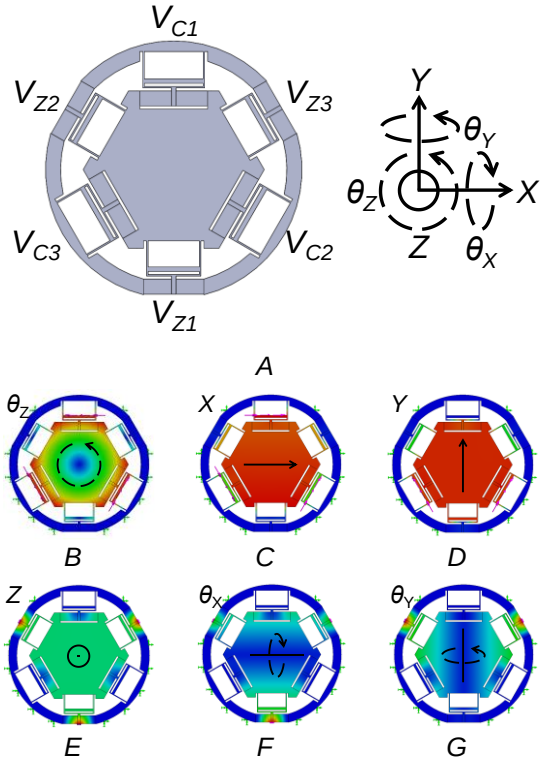

FIGURE 3. Top view (A) and simulated results (B - G) of the six-axis parallel flexural stage, demonstrating decoupled motions in all six axes

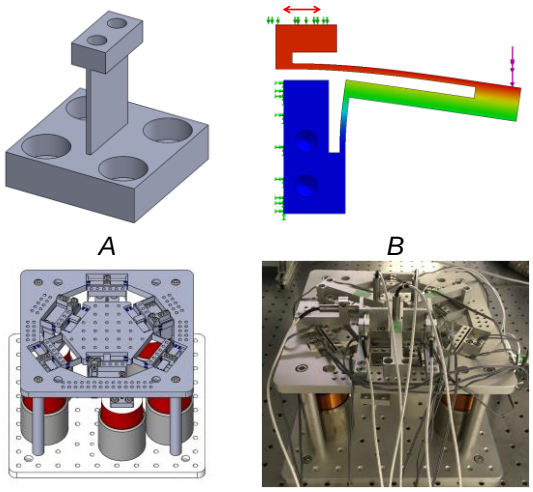

FIGURE 4. Decoupler for VCAs (A); motion steering mechanism (B) between the six-axis flexural stage and linear actuators; CAD model (C) and prototype (D) of the six-axis parallel nanopositioner

CHARACTERIZATION

To characterize the dynamic performance of the six-axis parallel positioner, an impulse response experiment has been conducted. Based on the measured displacement data from the capacitance probes, resonant frequencies in different axes are calculated by fast Fourier transform (FFT). Table 1 summarizes the performance specifications of the nanopositioner, including the resonant frequencies, strokes, and minimum step sizes in all six axes.

TABLE 1. Specifications of the six-axis parallel nanopositioner

	Freq.	Stroke	Min. step size
X	121 Hz	±80 μm	6 nm
Y	126 Hz	±60 μm	4 nm
Z	118 Hz	±70 μm	6 nm
θ_X	246 Hz	±900 μrad	150 nrad
θ_Y	216 Hz	±1700 μrad	120 nrad
θ_Z	188 Hz	±600 μrad	80 nrad

To characterize the cross-axis motion coupling effect, static displacement experiments were performed to identify the matrix, S_X, that maps the actuator input voltages, X_A, to the mechanism displacements, X_C. Six capacitance probes are fixed on a vibration isolation table to monitor the motions of the nanopositioner. Assuming small displacements, Eq. (1) and (2) can be used to obtain the matrix S_X [3]. The analytical solution of S_X is presented in Eq. (3), where a, b, c, d, e, f, g, and h are constant parameters related to the

characteristics of the VCAs and flexural stages. The analytical S_X indicates that the in-plane motions ($X/Y/\theta_Z$) and out-of-plane motions ($Z/\theta_X/\theta_Y$) are decoupled. Nevertheless, because of manufacturing errors and misaligned actuators and sensors, the measured S_X has deviations, and the motions in different axes are slightly coupled. The measured results are presented in Eq. (4). The units used in Eq. (1) - (4) are microns, microradians and millivolts.

$X_C = S_X X_A$, where

$$X_C = \begin{bmatrix} \Delta\theta_z & \Delta x & \Delta y & \Delta z & \Delta\theta_x & \Delta\theta_y \end{bmatrix}^{\mathrm{T}} \quad (1)$$

$$X_A = \begin{bmatrix} V_{C1} & V_{C2} & V_{C3} & V_{Z1} & V_{Z2} & V_{Z3} \end{bmatrix}^{\mathrm{T}}$$

$$X_A = S_X^{-1} X_C \quad (2)$$

$$S_X = \begin{bmatrix} a & a & a & 0 & 0 & 0 \\ -b & c & c & 0 & 0 & 0 \\ 0 & d & -d & 0 & 0 & 0 \\ 0 & 0 & 0 & e & e & e \\ 0 & 0 & 0 & -f & g & g \\ 0 & 0 & 0 & 0 & h & -h \end{bmatrix} \quad (3)$$

$$S_X = \begin{bmatrix} 0.158 & 0.154 & 0.149 & 0 & 0 & 0 \\ -0.029 & 0.008 & 0.008 & 0 & 0.013 & -0.015 \\ 0 & 0.020 & -0.020 & 0.012 & -0.009 & -0.009 \\ 0 & 0 & 0 & 0.015 & 0.021 & 0.021 \\ -0.128 & 0.067 & 0.073 & -0.401 & 0.273 & 0.299 \\ 0 & 0.139 & -0.109 & -0.030 & 0.450 & -0.480 \end{bmatrix} \quad (4)$$

POSITIONING EXPERIMENTS

We select the Z and θ_Z axes perform static positioning experiments for demonstrating the precision of the parallel positioner. In these experiments, the matrix, S_X^{-1}, is used in an open-loop controller, and the position signals are obtained from the six capacitance probes (C8/CPL190, Lion Precision, resolution: 20 nm). Figure 5 plots the measured displacements (left column) and off-axis errors (right column) versus open-loop displacement commands. The results show that the off-axis translational and rotational errors are reasonably small, i.e., within ±150 nm in $X/Y/Z$ axes, and ±3 μrad in $\theta_X/\theta_Y/\theta_Z$ axes. The precision can be further improved with closed-loop control.

Figure 6 presents the in-plane and out-of-plane positioning results for each axis under the PID control. In the experiments, the positioner is commanded to perform 1 μm and 10 μrad steps in the $X/Y/\theta_Z$ and $Z/\theta_X/\theta_Y$ axes in a sequential fashion, with each step held for about 15 seconds. As Fig. 6 shows, both in the in-plane and out-of-plane positioning experiments, the motion in one axis does not influence motions in other two axes. We have experimentally found that, under closed-loop control, the X, Y, Z, θ_X, θ_Y, and θ_Z axes have a resolution of 30 nm, 25 nm, 40 nm, 1.5 μrad, 1.4 μrad, and 1.0 μrad, respectively.

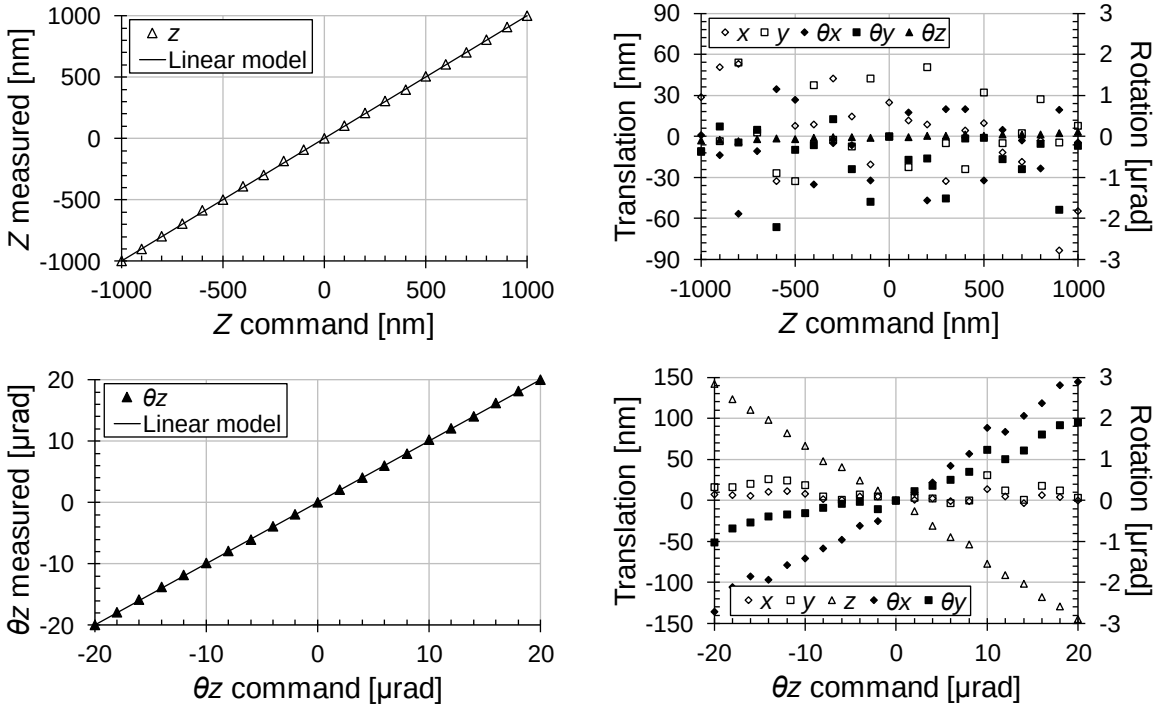

FIGURE 5. Z and θ_Z positioning results under open-loop control

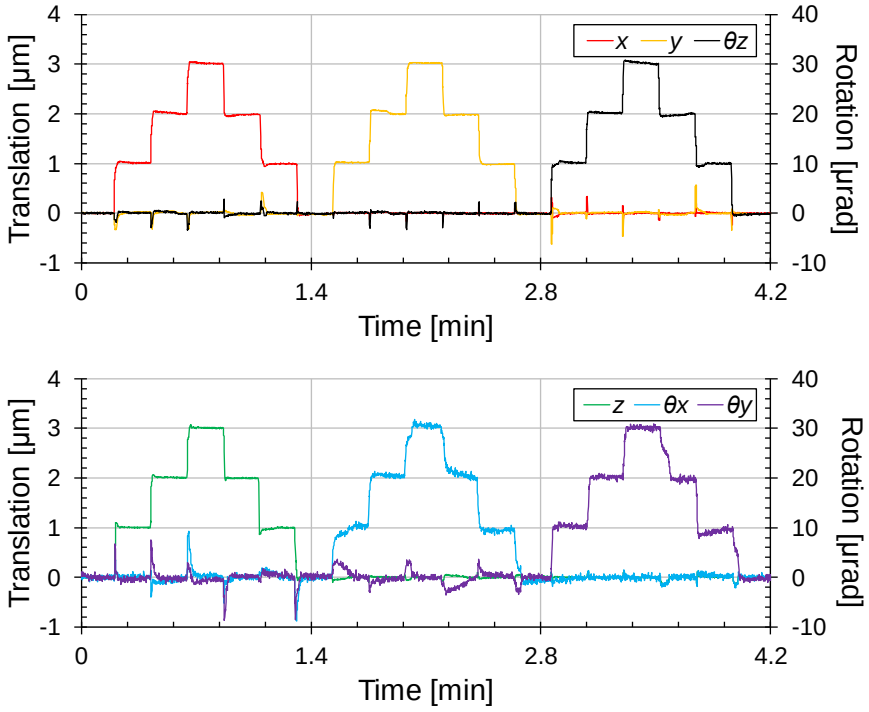

FIGURE 6. In-plane ($X/Y/\theta_Z$) and out-of-plane ($Z/\theta_X/\theta_Y$) positioning results, with PID control

CONCLUSION

We have presented the design and characterization of a flexure-based six-axis parallel positioner, demonstrating the new design method via combinations of decoupled flexural legs. The new six-axis parallel nanopositioner can be actuated by six linear VCAs and has decoupled in-plane and out-of-plane motions. Capacitance probes are used to monitor the displacement in all six axes in real time, and a resolution of ±40 nm in *X*/*Y*/*Z* axes, and ±1.5 µrad in $\theta_X/\theta_Y/\theta_Z$ axes has been achieved under closed-loop control. Dynamic performance of this flexural stage may be further improved by implementing deep learning-based control techniques [9].

ACKNOWLEDGMENT

This work is supported by the HKSAR Innovation and Technology Commission (ITC) Innovation and Technology Fund (ITF), ITS/077/17FP.

REFERENCES

[1] Howell L. Compliant Mechanisms. John Wiley and Sons Inc. New York: 2001.

[2] Blanding DL. Exact Constraint: Machine Design Using Kinematic Processing. ASME Press. New York: 1999.

[3] Culpepper ML, and Anderson G. Design of a Low-Cost Nano-Manipulator which Utilizes a Monolithic, Spatial Compliant Mechanism. Precision Engineering. 2004, 28(4), 469–482.

[4] Chen S, and Culpepper ML. Design of a Six-Axis Microscale Nanopositioner—µHexFlex. Precision Engineering. 2006, 30(3), 314–324.

[5] Stewart D. A Platform with Six Degrees of Freedom. Proceedings of the Institution of Mechanical Engineers. 1965, 180(1), 371–386.

[6] Wu T, Chen J, and Chang S. A Six-DOF Prismatic-Spherical-Spherical Parallel Compliant Nanopositioner. IEEE Transactions on Ultrasonics, Ferroelectrics, and Frequency Control. 2008, 55(12), 2544–2551.

[7] Li C, Wang J, and Chen S. Flexure-Based Dynamic-Tunable Five-Axis Nanopositioner for Parallel Nanomanufacturing. Precision Engineering. 2016, 45, 423–434.

[8] Awtar S, and Slocum AH. Constraint-Based Design of Parallel Kinematic XY Flexure Mechanisms. Journal of Mechanical Design. 2007, 129(8), 816–830.

[9] Liu X, Li C, and Chen S. Deep Learning-based Precision Control for Six-axis Compliant Nanopositioner. Proc. of the Annual Meeting of the ASPE, Pittsburgh, PA, USA, Oct. 2019.